

Angular and polarization properties of characteristic x-ray radiation following inner-shell $2p_{3/2}$ photoionization of high- Z atoms

Z. W. Wu ^{1,2,3,*}, W. Liu,¹ and S. Fritzsche ^{2,3,4}

¹Key Laboratory of Atomic and Molecular Physics and Functional Materials of Gansu Province, College of Physics and Electronic Engineering, Northwest Normal University, Lanzhou 730070, People's Republic of China

²Helmholtz-Institut Jena, Fröbelstieg 3, 07743 Jena, Germany

³GSI Helmholtzzentrum für Schwerionenforschung GmbH, Planckstrasse 1, 64291 Darmstadt, Germany

⁴Theoretisch-Physikalisches Institut, Friedrich-Schiller-Universität Jena, Max-Wien-Platz 1, 07743 Jena, Germany

 (Received 2 September 2023; revised 25 October 2023; accepted 1 November 2023; published 16 November 2023)

Inner-shell $2p_{3/2}$ photoionization of high- Z neutral atoms by linearly polarized light and subsequent $L\alpha_1$ ($3d_{5/2} \rightarrow 2p_{3/2}$), $L\alpha_2$ ($3d_{3/2} \rightarrow 2p_{3/2}$), and $L\ell$ ($3s_{1/2} \rightarrow 2p_{3/2}$) radiative decays are investigated within the framework of the density-matrix theory. Special attention is paid to angular and polarization behaviors of the radiated $L\alpha_1$, $L\alpha_2$, and $L\ell$ lines. To do this, relativistic single-configuration Dirac-Hartree-Fock calculations are performed for Ba, Yb, Hg, and Rn atoms with closed subshells. It is found that the $L\alpha_1$ line is nearly isotropic and that the $L\alpha_2$ and $L\ell$ lines are weakly anisotropic, behaviors that are rather different from the results predicted with nonrelativistic dipole approximations or analytical perturbation theory [V. K. Garg *et al.*, *J. Electron Spectrosc. Relat. Phenom.* **248**, 147054 (2021)]. In contrast, the polarization behaviors of these characteristic lines are found to be more promising for experimental implementation. To be specific, not only are the presently obtained linear polarizations of these lines strong enough to be measurable in experiment, but their dependences on the nuclear charge of atoms and ionizing photon energy are also noteworthy to be readily observed, in particular, for the weakest $L\ell$ line among them, which could be employed for exploring electron screening effect in inner-shell photoionization and decay dynamics of atoms.

DOI: [10.1103/PhysRevA.108.053115](https://doi.org/10.1103/PhysRevA.108.053115)

I. INTRODUCTION

Photoionization of atoms and ions is a fundamental atomic process in astrophysical and laboratory plasmas. In astrophysical plasmas near strong radiation sources, photoionization and photoexcitation often prevail over a variety of collisional processes and, in particular, inner-shell electrons of atoms and ions can become photoexcited or even photoionized due to the presence of energetic photons [1–4]. When one of the inner-shell electrons is photoionized by incident light, the resulting ions will reside in some excited hole states. These hole states are unstable and thus will decay radiatively or nonradiatively to some energetically lower states under the emission of characteristic photons or Auger electrons, respectively. Here special attention is paid to the emission of characteristic photons, which carries important information about electronic structure as well as excitation and decay dynamics of atoms or ions involved [5–9].

As early as half a century ago, Mehlhorn proposed theoretically for the first time that ionic hole states with total angular momentum larger than $1/2$ generated by electron or proton impact ionization are aligned and that the characteristic x-ray photons radiated from these aligned hole states should generally be polarized [10]. Since then, atomic physicists have been being interested in exploring the alignment of inner-shell hole

states following collisions of atoms or highly charged ions with (anti)protons, electrons, as well as ions. For example, alignment parameter values of the L_3 -subshell hole ($2p_{3/2}^{-1}$) states were derived and compared with theoretical results by measuring spectral intensities and anisotropy parameter values of characteristic x rays radiated following high-energy collisions of Au, Pb, and Bi atoms with energetic fluorine ions [11]. The effects of screened Coulomb interaction on the alignment of the $H(2p)$ state produced in collisions of H atoms with protons and antiprotons were studied for an energy range of 1–200 keV by using a two-center atomic orbital close-coupling method [12]. Furthermore, the effects of the Breit interaction on the alignment of the core-excited hole state $1s2s^22p_{1/2}$, $J = 1$ produced by resonant electron capture [13,14] and electron-impact excitation [15,16] of highly charged ions were investigated as well.

During the past decades, experimental and theoretical studies of the inner-shell photoionization of medium- and high- Z atoms have been attracting a great deal of attention owing to the fast development of strong light sources and corresponding experimental technologies [17,18]. As a matter of fact, a (nonzero) alignment of inner-shell-photoionized hole states can definitively give rise to an anisotropic and polarized emission behavior of characteristic photons, so the alignment of those photoionized hole states could be determined from angular distribution and polarization of emitted characteristic photons. Therefore, many studies have been carried out on angular distribution and linear polarization of characteristic

*zhongwen.wu@nwnu.edu.cn

photon emissions following photoionization of neutral atoms and highly charged ions. For example, Caldwell and Zare demonstrated that the excited doublet states $^2D_{3/2,5/2}$ of Cd^+ ions are aligned by measuring the degree of linear polarization of the resulting photon emissions following photoionization of cadmium [19], in which a theoretical calculation correctly predicted the sign of the degree of linear polarization though failed to reproduce the measured results. Karanfil and Barrea observed in experiment a nonisotropic angular distribution of the $L\alpha_1$ ($3d_{5/2} \rightarrow 2p_{3/2}$) and $L\alpha_2$ ($3d_{3/2} \rightarrow 2p_{3/2}$) lines following photoionization of Yb by a linearly polarized monochromatic photon beam, and the experimentally determined value of the alignment parameter shows very good agreement with the predicted theoretical result [20]. Alrakabi *et al.* determined experimentally the alignment of the L_3 -subshell vacancy states following photoionization of Au, Bi, Th, and U atoms by measuring the angular distribution of the subsequently emitted L_3 -subshell x rays, which clearly supports small theoretically predicted values of the alignment parameter, although it is difficult to deduce the predicted anisotropic trends [21]. In addition, Kämpfer *et al.* studied both experimentally and theoretically linear polarization of the $L\alpha_{1,2}$ lines following $2p_{3/2}$ photoionization of tungsten by unpolarized ionizing light, where the measured degree of linear polarization agrees very well with the theoretical results calculated within the electric dipole ($E1$) approximation [22]. Moreover, the influence of linearly polarized ionizing light on the linear polarization and angular distribution of the $L\alpha_{1,2}$ lines of the $2p_{3/2}$ -photoionized W^+ ions was also addressed [23].

Even though the $L\ell$ ($3s_{1/2} \rightarrow 2p_{3/2}$) line is the weakest among all the three $E1$ -allowed L_3 lines (i.e., $L\alpha_1$, $L\alpha_2$, and $L\ell$) and thus is paid little attention, it is expected to be more anisotropic and linearly polarized. Recently, Garg *et al.* studied angular distribution of the L_3 -subshell x rays following photoionization of high- Z W, Pt, Hg, Pb, and U atoms using several different theoretical schemes based on the nonrelativistic dipole approximation or the analytical perturbation theory [24]. It was found that the $L\ell$ line radiation behaves more anisotropically than the mixed $L\alpha$ one consisting of two subshell-resolved $L\alpha_{1,2}$ components with opposite anisotropy and also that both the $L\ell$ and $L\alpha$ lines are more anisotropic at the L_3 ionization threshold of all the atoms considered than a higher ionizing photon energy of 60 keV under all three theoretical schemes. Nevertheless, the calculated anisotropy values vary remarkably with the theoretical schemes used and at the L_3 threshold they are certainly larger than the reported experimental uncertainties of 5–8 % [24]. In the present work, a relativistic *ab initio* single-configuration Dirac-Hartree-Fock method is employed to investigate in detail the angular distribution and also linear polarization of the $L\alpha_{1,2}$ and $L\ell$ lines following $2p_{3/2}$ photoionization of high- Z atoms by linearly polarized light under the framework of the density-matrix theory.

The rest of this paper is structured as follows. In the following section we discuss the coordinates that are used to characterize the two-step inner-shell photoionization plus subsequent radiative decay of initially unpolarized atoms or ions. In Sec. III a density-matrix formalism is applied to study the angular distribution and linear polarization of characteristic

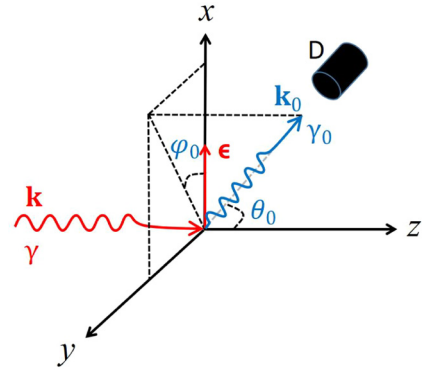


FIG. 1. Geometry describing the photoionization of atoms by linearly polarized light as well as subsequent radiative decay. The incident ionizing light γ propagates along the quantization z axis with its polarization vector ϵ along the x axis. The emission of characteristic γ_0 photons is characterized by the polar angle θ_0 and azimuthal angle φ_0 .

emission lines following photoionization. Then the presently obtained angular distribution and linear polarization of the $L\alpha_{1,2}$ and $L\ell$ lines are illustrated in Sec. IV and also compared with the results of Garg *et al.* [24]. A short summary is given in Sec. V.

II. GEOMETRY

Before formulating the inner-shell photoionization and subsequent radiative decay of atoms, an appropriate geometry should be specified first. To facilitate the formalism and simplify corresponding calculations, the quantization z axis is chosen to be along the wave vector \mathbf{k} of the incoming ionizing light γ , while the x axis is given by the direction of its polarization vector ϵ , from which the y axis is uniquely determined by a corresponding right-handed Cartesian coordinate system, as shown in Fig. 1. Under such a geometry, the emission of characteristic γ_0 photons with wave vector \mathbf{k}_0 is characterized by the polar angle θ_0 and azimuthal angle φ_0 .

III. THEORETICAL METHOD

To explore angular and polarization properties of characteristic photons following photoionization of atoms, a theoretical formalism based on the density-matrix theory [25,26] will be employed. Since this formalism has been introduced in detail in several works (for instance, Refs. [27,28]), below we just show the major steps for the considered inner-shell $2p_{3/2}$ photoionization by linearly polarized light and subsequent $L\alpha_{1,2}$ and $L\ell$ radiative decays, which is considered in practice to be a two-step process

$$\begin{aligned} A(\alpha_i J_i) + \gamma(h\nu) &\rightarrow A^+(\alpha_f J_f) + e^-(\epsilon l j) \\ &\rightarrow A^+(\alpha_0 J_0) + e^-(\epsilon l j) + \gamma_0. \end{aligned} \quad (1)$$

In the first step, one of the inner-shell $2p_{3/2}$ electrons of atom A in its ground state $|\alpha_i J_i\rangle$ is photoionized by an incoming ionizing photon $\gamma(h\nu)$, in which a resulting excited hole state $A^+(\alpha_f J_f)$ is formed. The subsequent radiative stabilization of the hole state to an energetically lower state $|\alpha_0 J_0\rangle$ in the

second step results in the emission of a characteristic (x-ray) photon γ_0 .

Within the density-matrix theory [25,26], the formation and decay of the hole state are treated separately. If the ionized photoelectron $e^-(\varepsilon l j)$ remains unobserved and the $E1$ approximation of the ionizing γ photon field is adopted, the statistical tensors $\rho_{kq}(\alpha_f J_f)$ of the photoionized $2p_{3/2}^{-1}$ hole state can be given under the geometry of Fig. 1 as [23]

$$\rho_{kq}(\alpha_f J_f) = 6\pi \sum_{lj} [2\langle 11, 1-1 | kq \rangle \delta_{0q} - (\delta_{2q} + \delta_{-2q}) \delta_{2k} P_\gamma] \times (-1)^{j+1/2} \begin{Bmatrix} 3/2 & j & 1 \\ 1 & k & 3/2 \end{Bmatrix} |T_{E1}^\gamma(\varepsilon l j)|^2, \quad (2)$$

which describes the relative population of magnetic substates of the $2p_{3/2}^{-1}$ hole state. Here the rank k of the statistical tensors $\rho_{kq}(2p_{3/2}^{-1}, J_f = 3/2)$ takes values of only 0 and 2 due to the total angular momentum $J_f = 3/2$ of the state and for each k its component q takes all integer values between $-k$ and k . Here l and j are the orbital and total angular momenta of the photoelectron, respectively, which are determined by the conservation laws of parity and total angular momentum of the ionizing system. The P_γ characterizes the linear polarization of the ionizing photon γ and is given by the first Stokes parameter. In addition, a shorthand notation $T_{E1}^\gamma(\varepsilon l j) \equiv \langle \alpha_f J_f = 3/2, \varepsilon l j : J \| H_{E1}^\gamma \| \alpha_i J_i \rangle$ for the reduced photoionization amplitudes and standard notations for the Clebsch-Gordan coefficients, the Wigner 6- j symbols, and the Kronecker delta functions are used. In practical applications, these statistical tensors ρ_{kq} are often renormalized with respect to the zero-rank tensor ρ_{00} as

$$\mathcal{A}_{kq}(\alpha_f J_f) = \frac{\rho_{kq}(\alpha_f J_f)}{\rho_{00}(\alpha_f J_f)}, \quad (3)$$

which are called reduced statistical tensors. In particular, the reduced second-rank tensors $\mathcal{A}_{2q}(\alpha_f J_f)$ are the so-called alignment parameters.

In order to formulate the angular distribution and linear polarization of the presently considered $L\alpha_{1,2}$ and $L\ell$ lines, we first need to obtain the (polarization) density matrix of the corresponding characteristic photons. Such a density matrix is generally expressed in the helicity representation instead of the spin angular momentum one, that is, $\langle \mathbf{k}_0 \lambda | \hat{\rho}_{\gamma_0} | \mathbf{k}_0 \lambda' \rangle$ with photon helicities $\lambda (\lambda') = \pm 1$. If the resulting ion $A^+(\alpha_0 J_0)$ after radiative decay is unobserved and again the $E1$ approximation of the radiation γ_0 field is employed, the (polarization) density matrix of the $L\alpha_{1,2}$ and $L\ell$ photons can be expressed as [23]

$$\begin{aligned} \langle \mathbf{k}_0 \lambda | \hat{\rho}_{\gamma_0} | \mathbf{k}_0 \lambda' \rangle &= 6\pi \sum_{kqq'} D_{-qq'}^k(\varphi_0, \theta_0, 0) \lambda \lambda' \rho_{kq}(\alpha_f J_f) \\ &\times (-1)^{J_0+k+q+1/2} \langle 1\lambda, 1-\lambda' | k-q' \rangle \\ &\times \begin{Bmatrix} 1 & 1 & k \\ 3/2 & 3/2 & J_0 \end{Bmatrix} |T_{E1}^{\gamma_0}(\alpha_0 J_0)|^2 \quad (4) \end{aligned}$$

in terms of the statistical tensors $\rho_{kq}(\alpha_f J_f)$ of the $2p_{3/2}^{-1}$ hole state given by Eq. (2). Here $D_{-qq'}^k(\varphi_0, \theta_0, 0)$ denotes the Wigner D matrix as a function of three Euler angles φ_0 , θ_0 , and 0, which relate the direction of the ionizing γ photon to that

of the emitted γ_0 photon by the three-step rotation. Moreover, the shorthand notation $T_{E1}^{\gamma_0}(\alpha_0 J_0) \equiv \langle \alpha_0 J_0 \| H_{E1}^{\gamma_0} \| \alpha_f J_f = 3/2 \rangle$ denotes the reduced amplitudes of the radiative $L\alpha_{1,2}$ and $L\ell$ decays.

As is well known, the (polarization) density matrix of any photons can be formally parametrized by means of the so-called Stokes parameters [25,26]. For the density matrix $\langle \mathbf{k}_0 \lambda | \hat{\rho}_{\gamma_0} | \mathbf{k}_0 \lambda' \rangle$ of the $L\alpha_{1,2}$ and $L\ell$ photons, such a parametrization has the form

$$\langle \mathbf{k}_0 \lambda | \hat{\rho}_{\gamma_0} | \mathbf{k}_0 \lambda' \rangle = \frac{W(\mathbf{k}_0)}{2} \begin{pmatrix} 1 + P_3 & -P_1 + iP_2 \\ -P_1 - iP_2 & 1 - P_3 \end{pmatrix}, \quad (5)$$

where $W(\mathbf{k}_0)$ is the total intensity (i.e., the angular distribution) of characteristic γ_0 photons emitted in the direction of \mathbf{k}_0 . The Stokes parameters P_1 and P_2 characterize linear polarization of the photons, while P_3 describes their circular polarization. In addition, it should be noted that the first and second lines (or columns) on the right-hand side of Eq. (5) correspond to the helicities $\lambda = +1$ and -1 , respectively.

In the present work we restrict ourselves to the angular distribution $W(\mathbf{k}_0)$ and the linear polarization $P_1(\mathbf{k}_0)$ of the $L\alpha_{1,2}$ and $L\ell$ photons, which can be easily formulated from Eq. (5) as

$$W(\mathbf{k}_0) = \langle \mathbf{k}_0, +1 | \hat{\rho}_{\gamma_0} | \mathbf{k}_0, +1 \rangle + \langle \mathbf{k}_0, -1 | \hat{\rho}_{\gamma_0} | \mathbf{k}_0, -1 \rangle \quad (6)$$

and

$$P_1(\mathbf{k}_0) = -\frac{\langle \mathbf{k}_0, +1 | \hat{\rho}_{\gamma_0} | \mathbf{k}_0, -1 \rangle + \langle \mathbf{k}_0, -1 | \hat{\rho}_{\gamma_0} | \mathbf{k}_0, +1 \rangle}{\langle \mathbf{k}_0, +1 | \hat{\rho}_{\gamma_0} | \mathbf{k}_0, +1 \rangle + \langle \mathbf{k}_0, -1 | \hat{\rho}_{\gamma_0} | \mathbf{k}_0, -1 \rangle}. \quad (7)$$

Here the (polarization) density-matrix elements appearing in Eqs. (6) and (7) are given by Eq. (4). In particular, if the emitted $L\alpha_{1,2}$ and $L\ell$ photons are measured in the reaction plane with the azimuthal angle $\varphi_0 = 0$, which is determined by the two propagation directions of the ionizing γ light and the emitted photons, the corresponding angular distribution $W(\mathbf{k}_0) \equiv W(\theta_0)$ of these characteristic photons can be explicitly expressed as follows with the use of Eqs. (2)–(6):

$$W(\theta_0) = 1 + \alpha_2^{\gamma_0} \sqrt{\frac{4\pi}{5}} \sum_{q=-2}^2 \mathcal{A}_{2q}(\alpha_f J_f) Y_{2q}(\theta_0, 0). \quad (8)$$

In this expression, $W(\theta_0)$ has been normalized with respect to the total intensity that is obtained by integrating over θ_0 . In addition, if the $L\alpha_{1,2}$ and $L\ell$ photons are measured perpendicular to the ionizing γ light (i.e., for $\theta_0 = \pi/2$ and $\varphi_0 = 0$), by means of Eqs. (2)–(5) and (7) the corresponding linear polarization $P_1(\mathbf{k}_0) \equiv P_1(\pi/2)$ can be written explicitly as

$$P_1 = \frac{\sqrt{\frac{3}{2}} \alpha_2^{\gamma_0} \sum_{q=-2}^2 2\mathcal{A}_{2q}(\alpha_f J_f) D_{q2}^{2*}(0, \pi/2, 0)}{1 + \alpha_2^{\gamma_0} \sqrt{\frac{4\pi}{5}} \sum_{q=-2}^2 \mathcal{A}_{2q}(\alpha_f J_f) Y_{2q}(\pi/2, 0)}. \quad (9)$$

In the expressions above, $Y_{2q}(\theta_0, \varphi_0)$ denotes the spherical harmonics. In addition, $\alpha_2^{\gamma_0}$ is the (so-called) intrinsic anisotropy parameters associated with the corresponding γ_0 photon emissions, which takes the values of $1/10$, $-2/5$, and $1/2$ for the presently considered dipole-allowed $L\alpha_{1,2}$ and $L\ell$ lines, respectively [26].

As seen from Eqs. (2)–(9), any further discussion of the angular distribution $W(\theta_0)$ and the linear polarization P_1 of

the characteristic $L\alpha_{1,2}$ and $L\ell$ lines simply needs to be traced back to the computation of the reduced $2p_{3/2}$ photoionization amplitudes $\langle \alpha_f J_f = 3/2, \varepsilon l j : J \| H_{E1}^\gamma \| \alpha_i J_i \rangle$ appearing in Eq. (2). The key to performing this is the generation of the continuum photoelectron wave function $|\mathbf{p}m_s\rangle$ with momentum \mathbf{p} and spin projection m_s , which is often decomposed into partial waves as [28–30]

$$|\mathbf{p}m_s\rangle = \sum_{\kappa m_j} i^l e^{-i\Delta_\kappa} \langle l m_l, 1/2 m_s | j m_j \rangle Y_{l m_l}^*(\hat{\mathbf{p}}) |\varepsilon l j m_j\rangle. \quad (10)$$

Note that in such a decomposition the spatial part of the photoelectron wave function has been rotated from the z axis to the $\hat{\mathbf{p}}$ direction since the quantization (z) axis is chosen along the wave vector \mathbf{k} of the incoming ionizing light γ in the present work. Furthermore, the summation in Eq. (10) runs over all possible partial waves, i.e., all possible values $\kappa = \pm 1, \pm 2, \dots$ of the Dirac angular momentum quantum number $\kappa = \pm(j + 1/2)$ for $l = j \pm 1/2$. The orbital angular momentum l indicates the parity $(-1)^l$ of the partial waves $|\varepsilon l j m_j\rangle$. In addition, Δ_κ represents the phase shift [31,32], which appears due to the (non-Coulombic) distortion potential of the nucleus and remaining electrons of the photoion [33]. In general, each of the partial waves $|\varepsilon l j m_j\rangle \equiv |\varepsilon \kappa m_j\rangle$ is further separated into the radial and angular form [30,34]

$$\langle r | \varepsilon \kappa m_j \rangle = \frac{1}{r} \begin{pmatrix} P_{\varepsilon \kappa}(r) \chi_{\kappa m_j} \\ i Q_{\varepsilon \kappa}(r) \chi_{-\kappa m_j} \end{pmatrix}, \quad (11)$$

in which $\chi_{\kappa m_j}$ represents the standard Dirac spin-angular function and the two (radial) wave functions $P_{\varepsilon \kappa}(r)$ and $Q_{\varepsilon \kappa}(r)$ are often called the large and small components, respectively, which can be obtained by solving the Dirac equation with consideration of the distortion potential. It is worth noting that when solving the differential equations of the two components, the phase shift is simultaneously determined, which depends only on the kinetic energy of the photoelectron [30,31]. Besides the photoelectron wave function $|\mathbf{p}m_s\rangle$, the reduced $2p_{3/2}$ photoionization amplitudes $\langle \alpha_f J_f = 3/2, \varepsilon l j : J \| H_{E1}^\gamma \| \alpha_i J_i \rangle$ still incorporate the $E1$ operator H_{E1}^γ . In the most general case, the (relativistic) electron-photon interaction is described by the transition operator $\hat{R}_\lambda(\mathbf{k}) = \sum_n \boldsymbol{\alpha}_n \cdot \mathbf{u}_\lambda e^{i\mathbf{k}\cdot\mathbf{r}_n}$, in which $\boldsymbol{\alpha}_n$ denotes the vector of the Dirac matrices for the n th electron and \mathbf{u}_λ is the polarization vector of the photon. This operator is often decomposed into the form of multipole components in practical calculations. If the quantization axis is chosen along the ionizing photon momentum, as done in the present work, such a decomposition reads [35]

$$\begin{aligned} \mathbf{u}_\lambda e^{i\mathbf{k}\cdot\mathbf{r}_n} &= \sqrt{2\pi} \sum_L i^L \sqrt{2L+1} (\mathbf{A}_{L\lambda}^{(m)} + i\lambda \mathbf{A}_{L\lambda}^{(e)}) \\ &\equiv \sqrt{2\pi} \sum_L \sum_{p=0,1} i^L \sqrt{2L+1} (i\lambda)^p \mathbf{A}_{L\lambda}^p. \end{aligned} \quad (12)$$

Here the denotations $\mathbf{A}_{L\lambda}^{(e)} \equiv \mathbf{A}_{L\lambda}^{p=1}$ and $\mathbf{A}_{L\lambda}^{(m)} \equiv \mathbf{A}_{L\lambda}^{p=0}$ are used for the electric ($p=1$) and magnetic ($p=0$) multipole fields, respectively. Based on the above considerations, the reduced $2p_{3/2}$ photoionization amplitudes can be written more

TABLE I. Presently calculated inner-shell $2p_{3/2}$ ionization energies (in units of eV) of Ba ($Z=56$), Yb ($Z=70$), Hg ($Z=80$), and Rn ($Z=86$) atoms with closed subshells, compared with other theoretical and experimental results [39,40]. Numbers in parentheses are one standard deviation uncertainties of the quoted value referring to its last figures.

Work	Ba	Yb	Hg	Rn
present	5256.30	8943.87	12292.66	14620.78
Ref. [39] ^a	5257.36(32)	8944.26(35)	12292.28(39)	14619.53(43)
Ref. [39] ^b	5247.04(33)	8944.04(95)	12286.4(18)	
Ref. [40]	5247.0(3)	8943.6(4)	12283.9(4)	14619.4(30)

^aCalculated ionization energies from Ref. [39].

^bConverted from the experimental data of Ref. [40].

explicitly as

$$\begin{aligned} \langle \alpha_f J_f = 3/2, \varepsilon l j : J \| H_{E1}^\gamma \| \alpha_i J_i \rangle \\ = i^{-l} e^{i\Delta_\kappa} \langle \alpha_f J_f = 3/2, \varepsilon l j : J \| \sum_n \boldsymbol{\alpha}_n \cdot \mathbf{u}_\lambda e^{i\mathbf{k}\cdot\mathbf{r}_n} \| \alpha_i J_i \rangle, \end{aligned} \quad (13)$$

which will be further simplified with the use of Eq. (12) and the $E1$ approximation (i.e., $p=1$ and $L=1$ therein). In the present work, all of the required energy levels and wave functions as well as the $2p_{3/2}$ photoionization amplitudes were calculated within a single-configuration Dirac-Hartree-Fock approximation [36] using the GRASP2018 [37] and the RATIP [38] packages, which was shown in our previous work [22] to be sufficient to properly reproduce high-precision experimental measurement for inner-shell $2p_{3/2}$ photoionization of high- Z atoms as considered presently.

IV. RESULTS AND DISCUSSION

In Table I we list the presently calculated $2p_{3/2}$ ionization energies of selected high- Z Ba ($Z=56$), Yb ($Z=70$), Hg ($Z=80$), and Rn ($Z=86$) atoms, which are compared with other theoretical and experimental results available from the literature [39,40]. Note that there are two sets of data relevant to Ref. [39], one set for the calculated ionization energies and another set for the converted values from the experimental ionization energies of Ref. [40] with certain conversion factors listed in Ref. [39]. As seen clearly from Table I, the present $2p_{3/2}$ ionization energies are in excellent agreement with these available results. To be more specific, the relative discrepancies are found to be within 0.18% for all these high- Z atoms considered, which shows to some extent the reliability of wave functions and energy levels involved in the subsequent computation of the reduced $2p_{3/2}$ photoionization amplitudes.

Before showing the experimentally measurable angular distribution and linear polarization of the $L\alpha_{1,2}$ and $L\ell$ lines, let us first discuss briefly the alignment parameters $\mathcal{A}_{2q}(2p_{3/2}^{-1}, J_f = 3/2)$ of the photoionized $2p_{3/2}^{-1}$ state even if, for the sake of brevity, their values are not listed explicitly here. As for the presently considered $2p_{3/2}$ photoionization of (unpolarized) atoms by linearly polarized light with $P_\gamma = \pm 1$, only \mathcal{A}_{20} and $\mathcal{A}_{2\pm 2}$ with components 0 and ± 2 are nonzero. Furthermore, the parameter \mathcal{A}_{22} is found to be fully identical

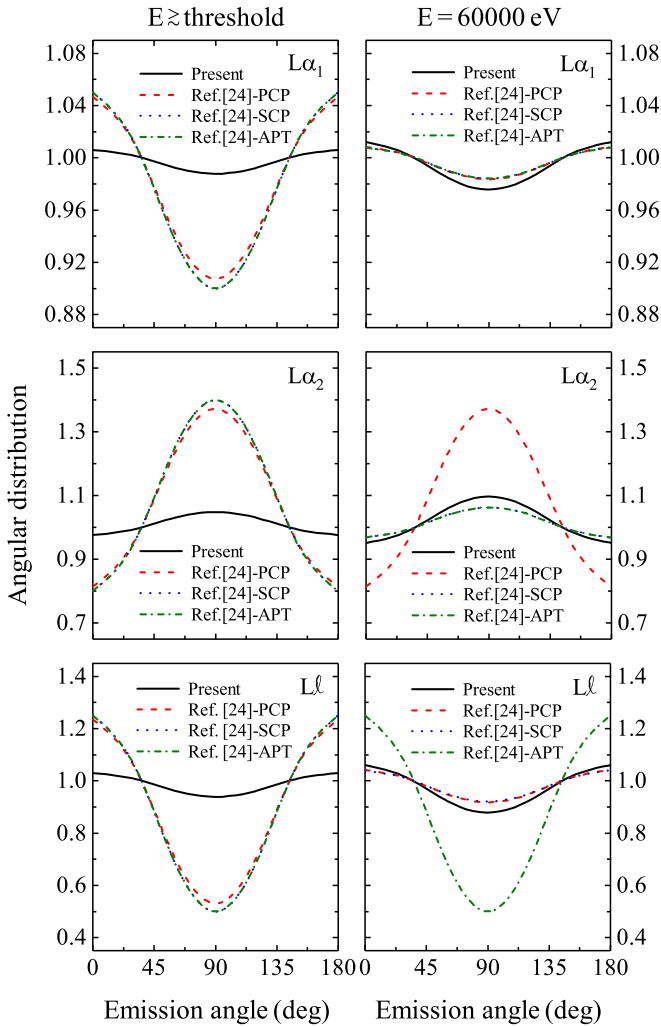


FIG. 2. Comparison of the presently calculated angular distribution $W(\theta_0)$ (black solid lines) of the $L\alpha_1$ (top row), $L\alpha_2$ (middle), and Ll (bottom) lines following $2p_{3/2}$ photoionization of Hg atoms by linearly polarized light with $P_\gamma = 1$ with other nonrelativistic or analytical results calculated using the PCP (red dashed lines), SCP (blue dotted lines), and APT (green dash-dotted lines) schemes by Garg *et al.* [24]. Results are presented for two ionizing γ photon energies: the $2p_{3/2}$ ionization threshold (left column) and 60 000 eV (right).

to the parameter \mathcal{A}_{2-2} owing to spatial symmetry of the $2p_{3/2}^{-1}$ hole state produced under the geometry as shown in Fig. 1. This is also indicated by the present calculations performed for different ionizing photon energies and polarizations.

Figure 2 displays the presently obtained angular distribution of the $L\alpha_{1,2}$ and Ll lines following $2p_{3/2}$ photoionization of Hg atoms by linearly polarized light with $P_\gamma = 1$, along with the results of Garg *et al.* calculated by using three theoretical schemes for comparison, that is, two nonrelativistic dipole approximations with point Coulomb potential (PCP) and with screened Coulomb potential (SCP), respectively, as well as an analytical perturbation theory (APT) [24]. Results are plotted for two different ionizing photon energies, i.e., the $2p_{3/2}$ ionization threshold 12 292.66 eV and a higher energy of 60 000 eV. It should be noted that for the calculation of the

angular distribution at the $2p_{3/2}$ ionization threshold the actual ionizing photon energy is taken to be slightly higher than the threshold by a few eV to avoid numerical difficulties resulting from photoelectrons with zero kinetic energy, as we did for electron-impact excitation of ions at the excitation threshold [8,41,42], which will be adopted for other atoms considered below. The present results show that at both ionizing energies considered the $L\alpha_1$ line is radiated almost isotropically, while the $L\alpha_2$ and Ll lines are both weakly anisotropic but with an opposite angular emission pattern, which is rather different from the results predicted by Garg *et al.* using the PCP, SCP, and APT schemes [24]. To be more specific, at the ionization threshold energy the anisotropies of the three characteristic lines are all overestimated remarkably by Garg *et al.* when compared to the present findings. However, at the ionizing photon energy of 60 000 eV, the consistencies of the angular distribution among different calculations behave very differently for the $L\alpha_{1,2}$ and Ll lines. First of all, for the $L\alpha_1$ line the presently obtained angular distribution agrees very well with all the results from the PCP, SCP, and APT schemes, although it is almost isotropic. As for the $L\alpha_2$ line, the present calculation shows that it is preferentially radiated perpendicularly to the incoming ionizing light (i.e., $\theta_0 = \pi/2$ and $\varphi_0 = 0$), which coincides well with the SCP and APT results, whereas in contrast the PCP scheme predicted a much more anisotropic angular distribution. With respect to the characteristic Ll line, a forward- and backward-dominated radiation pattern is obtained in the present calculation, which also agrees well with the PCP and SCP results of Garg *et al.* but behaves much less anisotropically than their APT result. Overall, for all three $E1$ -allowed lines, although large discrepancies are obtained between the present relativistic *ab initio* results and the nonrelativistic or analytical PCP, SCP, and APT results of Garg *et al.* [24], all of them give rise to the same emission pattern (that is, the sign of the anisotropies) for each of the lines at both ionizing photon energies.

In addition to Hg atoms, we further analyze the angular distributions of the $L\alpha_{1,2}$ and Ll lines following $2p_{3/2}$ photoionization of high- Z Ba, Yb, and Rn atoms by linearly polarized light γ with $P_\gamma = 1$, which are illustrated in Fig. 3. Once again, for each of these atoms the results are calculated for two ionizing photon energies, that is, their respective $2p_{3/2}$ ionization thresholds as listed in Table I and an energy of 60 000 eV. It is found that the presently obtained angular distributions of the $L\alpha_{1,2}$ and Ll lines for Ba, Yb, and Rn atoms are nearly the same as for Hg atoms, which indicates that for heavy neutral atoms ($56 \leq Z \leq 86$) the number of outer-shell electrons beyond the $2p_{3/2}$ subshell hardly affects the alignment of the photoionized $2p_{3/2}^{-1}$ hole state and the angular behavior of the subsequent $L\alpha_{1,2}$ and Ll radiative decays. For the case of $P_\gamma = -1$, the angular distributions of all the $L\alpha_{1,2}$ and Ll lines are found to be completely isotropic and thus are not presented here. Such an isotropic distribution can be illustratively understood as follows. Under the considered geometry as shown in Fig. 1, $P_\gamma = -1$ means that the ionizing light γ is linearly polarized along the y axis and, as a consequence, the photoionized $2p_{3/2}^{-1}$ hole state is certainly aligned along the same y direction. Within the $E1$ approximation of the ionizing and radiation fields, only this direction is physically significant. Since the angular

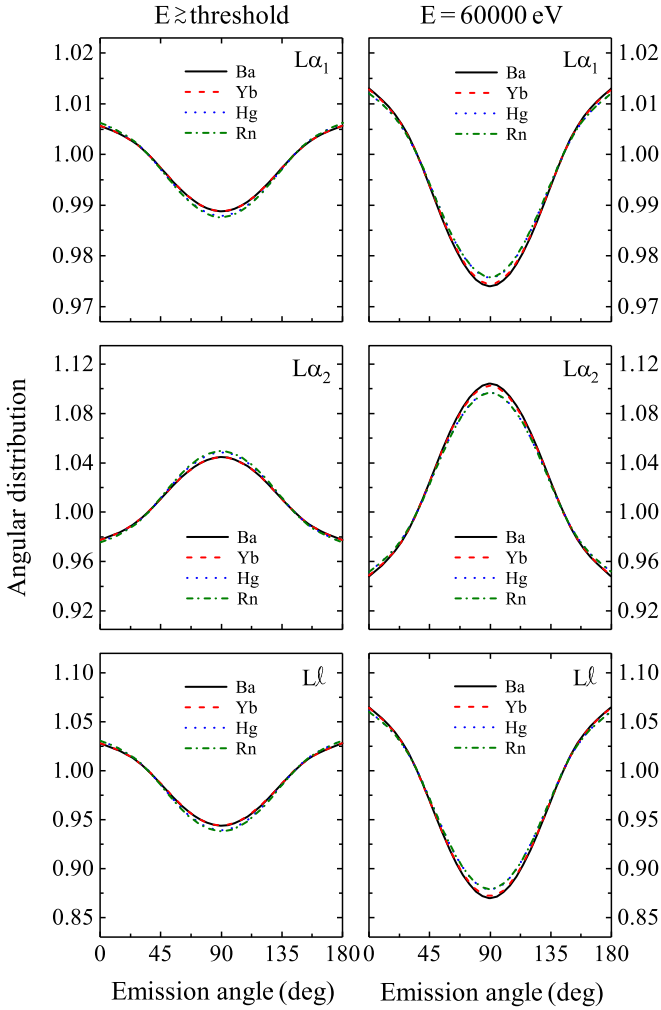


FIG. 3. Angular distribution $W(\theta_0)$ of the $L\alpha_1$ (top row), $L\alpha_2$ (middle), and $L\ell$ (bottom) lines following $2p_{3/2}$ photoionization of Ba (black solid lines), Yb (red dashed lines), Hg (blue dotted lines), and Rn (green dash-dotted lines) atoms by linearly polarized γ light with $P_\gamma = 1$. Again, results are shown for two ionizing photon energies: their respective $2p_{3/2}$ ionization thresholds (left column) and 60 000 eV (right).

distribution of these characteristic lines is considered in the reaction plane that is perpendicular to the y axis, they are destined to be completely isotropic.

Apart from the angular properties of the characteristic $L\alpha_{1,2}$ and $L\ell$ lines, as studied by Garg *et al.* [24], we also explore their polarization properties, which might be more interesting and promising for forthcoming measurements. For example, Fig. 4 displays the linear polarization P_1 of the $L\alpha_{1,2}$ and $L\ell$ lines radiated perpendicularly to the ionizing light (i.e., $\theta_0 = \pi/2$) following $2p_{3/2}$ photoionization of Ba, Yb, Hg, and Rn atoms by linearly polarized light with $P_\gamma = -1$, as functions of ionizing photon energy in units of their respective ionization thresholds as tabulated in Table I. As seen from the figure, the $L\ell$ line is the most linearly polarized among the three lines at any given ionizing photon energies for each of the atoms, which is followed by the $L\alpha_2$ and $L\alpha_1$ lines in sequence. In contrast to the angular distribution as discussed above, the linear polarization P_1 is found to be remarkably

dependent upon the nuclear charge of atoms and also upon the ionizing photon energy for each of the $L\alpha_{1,2}$ and $L\ell$ lines, respectively, which is more physically significant. The $L\alpha_{1,2}$ and $L\ell$ lines radiated from atoms with higher nuclear charge are more linearly polarized for the ionizing photon energies considered, and such a characteristic becomes more prominent at higher photon energies. Moreover, for each of the atoms the linear polarization P_1 of the $L\alpha_{1,2}$ and $L\ell$ lines becomes stronger with the increase of the ionizing γ photon energy. Take the $L\ell$ line as an example: The linear polarization P_1 increases from 9.3% for Ba ($Z = 56$) atoms to 10.6% for Rn ($Z = 86$) atoms at the ionizing photon energy of 1.1 times their respective ionization thresholds, while it changes from 12.9% to 16.7% at an energy of 4.0 times their respective thresholds. In addition, for the case of $P_\gamma = 1$ all these lines considered are found to be fully unpolarized. Such a result is the consequence of the choice of the present geometry. To be specific, $P_\gamma = 1$ means that the ionizing light γ is linearly polarized along the x axis and thus the photoionized $2p_{3/2}^{-1}$ hole state is aligned along the same x direction. Since the linear polarization P_1 of these characteristic lines is calculated for those photons emitted in the direction of $\theta_0 = \pi/2$ and $\varphi_0 = 0$ (that is, along the x axis) and photons are transversely polarized in nature, the linear polarization P_1 must be zero under the geometry considered. Finally, it is worth mentioning that the presently obtained linear polarization P_1 of the $L\alpha_2$ and $L\ell$ lines for the case of $P_\gamma = -1$ and its dependences upon the nuclear charge and also upon the ionizing photon energy are strong enough to be measurable using present-day (crystal-based) x-ray polarimeters [43] or microcalorimeters [44,45], although it is insignificant to observe their nearly isotropic angular distributions as discovered above.

V. CONCLUSION

To summarize, in light of the work of Garg *et al.* [24], the inner-shell $2p_{3/2}$ photoionization of atoms by linearly polarized ionizing light with $P_\gamma = \pm 1$ and the subsequent $L\alpha_{1,2}$ and $L\ell$ radiative decays have been investigated within the framework of the density-matrix theory. Apart from angular emission behaviors of these $E1$ -allowed characteristic lines, as explored by Garg *et al.* using the nonrelativistic dipole approximations or analytical perturbation theory, we paid particular attention to their polarization properties as well. To do so, detailed relativistic single-configuration Dirac-Hartree-Fock calculations were done for selected high- Z Ba, Yb, Hg, and Rn atoms with closed subshells for the sake of simplicity. By using the presently calculated reduced $2p_{3/2}$ photoionization amplitudes, the second-rank alignment parameters A_{2q} of the photoionized $2p_{3/2}^{-1}$ hole state and further the angular distribution and linear polarization P_1 of the $L\alpha_{1,2}$ and $L\ell$ lines were obtained. It was found that the $L\alpha_1$ line is nearly isotropic and the $L\alpha_2$ and $L\ell$ lines are weakly anisotropic, which is insignificant and rather different from the results of Garg *et al.* [24]. In contrast, the linear polarization of these characteristic lines was found to be more significant for experimental implementation; not only is it known to be strong enough to be measurable in experiment, but its dependences on both the nuclear charge of atoms and ionizing photon energy are also noteworthy to be readily observed, in particular,

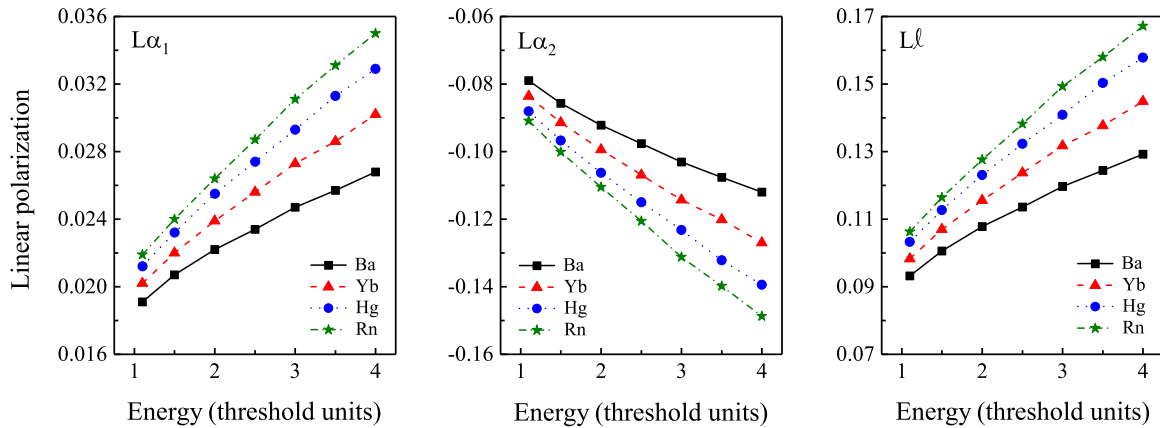


FIG. 4. Linear polarization P_1 of the characteristic $L\alpha_1$ (left panel), $L\alpha_2$ (middle), and $L\ell$ (right) lines radiated perpendicularly to the incoming ionizing light (that is, $\theta_0 = \pi/2$ and $\varphi_0 = 0$) following $2p_{3/2}$ photoionization of Ba (black solid lines with squares), Yb (red dashed lines with triangles), Hg (blue dotted lines with circles), and Rn (green dash-dotted lines with stars) atoms by linearly polarized light with $P_y = -1$, as functions of ionizing photon energy in the range from 1.1 to 4.0 times their respective ionization thresholds as listed in Table I.

for the weakest $L\ell$ line among them. In the end, it is worth mentioning that the presently obtained linear polarization P_1 of these characteristic lines and the discovered dependences are measurable with the use of state-of-the-art x-ray polarimeters or microcalorimeters, which could be expected to be employed in exploring the electron screening effect in inner-shell photoionization and radiative decay dynamics of atoms.

ACKNOWLEDGMENTS

This work was supported by the National Natural Science Foundation of China under Grants No. 12174315 and

No. 11804280, the Chinese Scholarship Council under Grant No. 202008620004, the Youth Science and Technology Talent Promotion Project of Gansu Province under Grant No. GXH2020626-09, the Longyuan Youth Innovation and Entrepreneurship Talent Project of Gansu Province under Grant No. 2021LQGR64, the Outstanding Youth Fund of the Science and Technology Project of Gansu Province under Grant No. 23JRRA687, and the Key Program of the Research Ability Promotion Project for Young Scholars of Northwest Normal University under Grant No. NWNLU-LKQN2019-5. Z.W.W. is sincerely grateful to the anonymous referees for their constructive suggestions and comments on this work.

- [1] G. Sarkar, D. A. García-Hernández, M. Parthasarathy, A. Manchado, P. García-Lario, and Y. Takeda, *Mon. Not. R. Astron. Soc.* **421**, 679 (2012).
- [2] E. Ripamonti and M. Mapelli, *Mon. Not. R. Astron. Soc.* **423**, 1144 (2012).
- [3] D. A. Berg, D. K. Erb, M. W. Auger, M. Pettini, and G. B. Brammer, *Astrophys. J.* **859**, 164 (2018).
- [4] D. Baron, H. Netzer, J. X. Prochaska, Z. Cai, S. Cantalupo, D. C. Martin, M. Matuszewski, A. M. Moore, P. Morrissey, and J. D. Neill, *Mon. Not. R. Astron. Soc.* **480**, 3993 (2018).
- [5] S. Fritzsche, A. Surzhykov, A. Gumberidze, and T. Stöhlker, *New J. Phys.* **14**, 083018 (2012).
- [6] Z. W. Wu, A. Surzhykov, and S. Fritzsche, *Phys. Rev. A* **89**, 022513 (2014).
- [7] Z. W. Wu, A. V. Volotka, A. Surzhykov, C. Z. Dong, and S. Fritzsche, *Phys. Rev. A* **93**, 063413 (2016).
- [8] Z. W. Wu, Z. Q. Tian, J. Jiang, C. Z. Dong, and S. Fritzsche, *Phys. Rev. A* **104**, 062814 (2021).
- [9] Z. W. Wu, Z. M. He, Z. Q. Tian, C. Z. Dong, and S. Fritzsche, *Phys. Rev. A* **105**, 062813 (2022).
- [10] W. Mehlhorn, *Phys. Lett. A* **26**, 166 (1968).
- [11] A. Kumar, A. N. Agnihotri, D. Misra, S. Kasthurirangan, L. Sarkadi, and L. C. Tribedi, *J. Phys. B* **45**, 215205 (2012).
- [12] D. Jakimovski and R. K. Janev, *Eur. Phys. J. D* **70**, 153 (2016).
- [13] S. Fritzsche, A. Surzhykov, and T. Stöhlker, *Phys. Rev. Lett.* **103**, 113001 (2009).
- [14] Z. Hu, X. Han, Y. Li, D. Kato, X. Tong, and N. Nakamura, *Phys. Rev. Lett.* **108**, 073002 (2012).
- [15] Z. W. Wu, M. M. Zhao, C. Ren, C. Z. Dong, and J. Jiang, *Phys. Rev. A* **101**, 022701 (2020).
- [16] Z. W. Wu, Y. Li, Z. Q. Tian, and C. Z. Dong, *Phys. Rev. A* **105**, 032809 (2022).
- [17] J. M. J. Madey, *J. Appl. Phys.* **42**, 1906 (1971).
- [18] T. Ishikawa *et al.*, *Nat. Photon.* **6**, 540 (2012).
- [19] C. D. Caldwell and R. N. Zare, *Phys. Rev. A* **16**, 255 (1977).
- [20] C. Karanfil and R. A. Barrea, *J. Phys. B* **44**, 235002 (2011).
- [21] M. Alrakabi, S. Kumar, V. Sharma, G. Singh, and D. Mehta, *Eur. Phys. J. D* **67**, 99 (2013).
- [22] T. Kämpfer, I. Uschmann, Z. W. Wu, A. Surzhykov, S. Fritzsche, E. Förster, and G. G. Paulus, *Phys. Rev. A* **93**, 033409 (2016).
- [23] D. H. Zhang, C. Z. Dong, and Z. W. Wu, *J. Quant. Spectrosc. Radiat. Transfer* **244**, 106844 (2020).
- [24] V. K. Garg, R. Mittal, and A. Sharma, *J. Electron Spectrosc. Relat. Phenom.* **248**, 147054 (2021).

- [25] K. Blum, *Density Matrix Theory and Applications*, 3rd ed. (Springer, Berlin, 2012).
- [26] V. V. Balashov, A. N. Grum-Grzhimailo, and N. M. Kabachnik, *Polarization and Correlation Phenomena in Atomic Collisions* (Kluwer Academic, New York, 2000).
- [27] N. Kabachnik, S. Fritzsche, A. Grum-Grzhimailo, M. Meyer, and K. Ueda, *Phys. Rep.* **451**, 155 (2007).
- [28] L. Sharma, A. Surzhykov, M. K. Inal, and S. Fritzsche, *Phys. Rev. A* **81**, 023419 (2010).
- [29] M. K. Inal, A. Surzhykov, and S. Fritzsche, *Phys. Rev. A* **72**, 042720 (2005).
- [30] J. Eichler and W. E. Meyerhof, *Relativistic Atomic Collisions* (Academic, San Diego, 1995).
- [31] R. H. Pratt, A. Ron, and H. K. Tseng, *Rev. Mod. Phys.* **45**, 273 (1973).
- [32] H. K. Tseng, R. H. Pratt, S. Yu, and A. Ron, *Phys. Rev. A* **17**, 1061 (1978).
- [33] S. Fritzsche, A. Surzhykov, and T. Stöhlker, *Phys. Rev. A* **72**, 012704 (2005).
- [34] V. B. Berestetskii, E. M. Lifshitz, and L. P. Pitaevskii, *Relativistic Quantum Theory* (Pergamon, Oxford, 1971).
- [35] M. E. Rose, *Elementary Theory of Angular Momentum* (Wiley, New York, 1957).
- [36] I. P. Grant, *Relativistic Quantum Theory of Atoms and Molecules: Theory and Computation* (Springer, New York, 2007).
- [37] C. F. Fischer, G. Gaigalas, P. Jönsson, and J. Bieroń, *Comput. Phys. Commun.* **237**, 184 (2019).
- [38] S. Fritzsche, *Comput. Phys. Commun.* **183**, 1525 (2012).
- [39] R. D. Deslattes, E. G. Kessler, P. Indelicato, L. de Billy, E. Lindroth, and J. Anton, *Rev. Mod. Phys.* **75**, 35 (2003).
- [40] J. A. Bearden and A. F. Burr, *Rev. Mod. Phys.* **39**, 125 (1967).
- [41] Z. W. Wu, Z. Q. Tian, J. Jiang, C. Z. Dong, and S. Fritzsche, *Phys. Rev. A* **102**, 042813 (2020).
- [42] Z. W. Wu, Z. Q. Tian, Y. H. An, and C. Z. Dong, *Astrophys. J.* **910**, 142 (2021).
- [43] B. Marx, K. S. Schulze, I. Uschmann, T. Kämpfer, R. Löttsch, O. Wehrhan, W. Wagner, C. Detlefs, T. Roth, J. Härtwig *et al.*, *Phys. Rev. Lett.* **110**, 254801 (2013).
- [44] C. Pies, S. Schäfer, S. Heuser, S. Kempf, A. Pabinger, J. Porst, P. Ranitsch, N. Foerster, D. Hengstler, A. Kampkötter *et al.*, *J. Low Temp. Phys.* **167**, 269 (2012).
- [45] S. Kraft-Bermuth, V. Andrianov, A. Bleile, A. Echler, P. Egelhof, P. Grabitz, S. Ilieva, O. Kiselev, C. Kilbourne, D. McCammon *et al.*, *J. Phys. B* **50**, 055603 (2017).